



International Journal of Control Theory and Applications

ISSN : 0974-5572

© International Science Press

Volume 10 • Number 25 • 2017

Lung Segmentation using Rotational Wavelet Gabour Filter

Afshan Khanum^a, Purushothaman S.^b and Rajeswari P.^c

^aResearch Scholar, Department of Computer Science and Engineering, VELS University, Chennai, India-600117. Email: afshankhanum2013@gmail.com

^bChennai, India. Email: dr.s.purushothaman@gmail.com

^cDepartment of Computer Science, Girls Community College, King Khalid University, Abha, Saudi Arabia. Email: dr.p.rajeswari@gmail.com

Abstract: This paper presents the implementation of rotational wavelet Gabor filter for segmentation of lung images. Images are collected from early lung cancer action program (ELCAP) database. A lung image is preprocessed and subsequently segmented by using Gabor filter. The segmented image contains white patches. The segmentation accuracy of the implemented algorithm is presented for four different images.

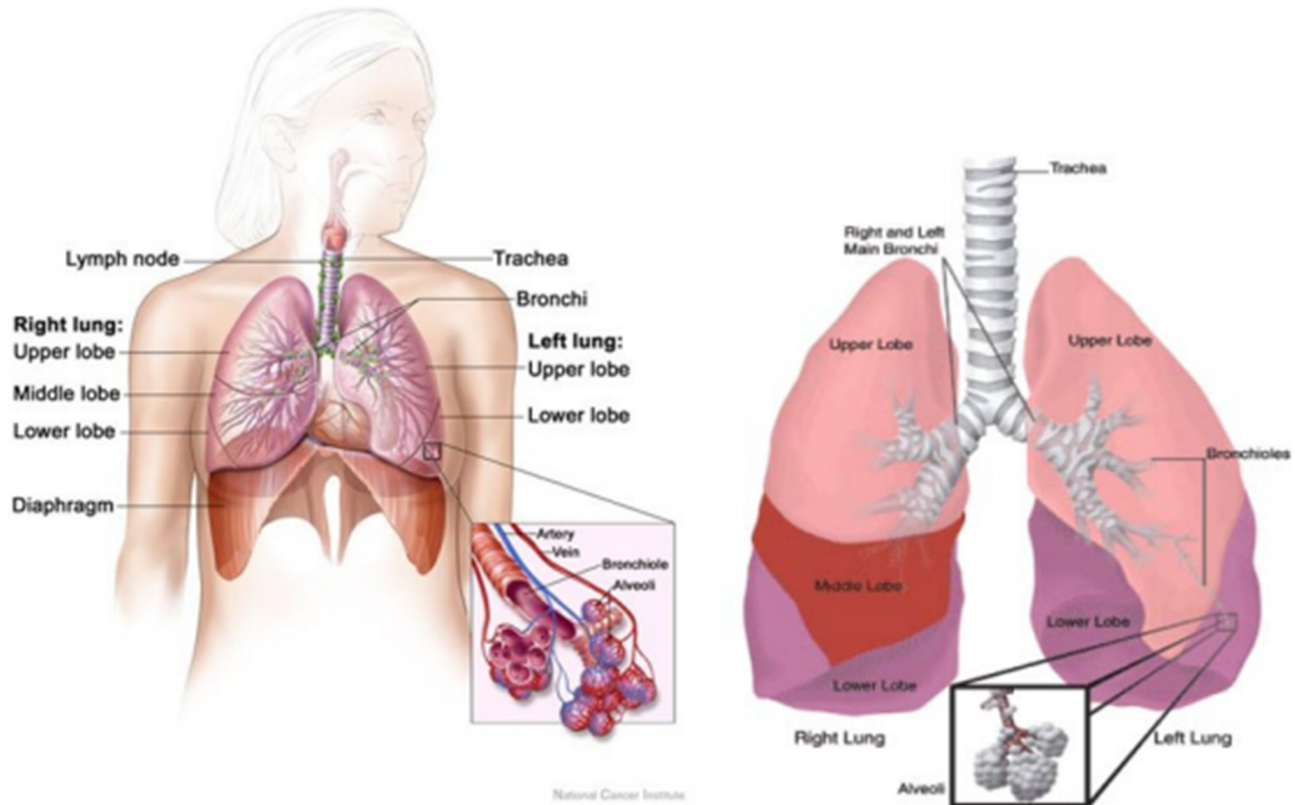
Keywords: ELCAP database; segmentation; Lung; Rotational Gabor wavelet.

1. INTRODUCTION

Lung nodules represent lung abnormalities. Lung pulmonary nodules are spherical in shape with high density. Large malignant nodules with a diameter greater than 1cm can be detected using the traditional imaging equipment easily.

A nodule can be solid, non-solid or partly solid; and soft tissue or Ground-Glass Opacity (GGO) which is less than 3cm diameter. Chest image processing is a good approach for effective pulmonary image analysis. The computed tomography (CT) images have been used by many radiologists for the diagnosis of various pulmonary diseases such as lung cancer, Tuberculosis, and Pulmonary embolism.

The lungs are a pair of involuntary organs present in the chest which perform a multitude of various important functions in each and every second of our lives. Breathing is an essential operation for these functions in which the lungs take the oxygen from the atmosphere, transports it into the bloodstream and removes the carbon dioxide from the bloodstream towards the atmosphere. Human lungs are branched into right and left lungs. The left lung is divided into two lobes and the right into three lobes. The tissues present in the lungs are spongy in nature due to the presence of gas-filled cavities called alveoli. The anatomy of human lungs is shown in Figure 1. There are about 250-350 million alveoli in an adult lung. The lungs play a vital role in the body's defensive mechanism against the infection and other harmful environmental factors.



(a) Source: www.yourcancertoday.com

(b) Source: www.cancerline.com

Figure 1: Anatomy of Human Lungs

Lung cancer is caused by the rapid growth and division of cells which takes place in the formation of lungs. The lung cancer can be classified into two major categories namely primary lung cancer and secondary (metastatic) lung cancer. The primary lung cancer originates in the cells of the lungs, while secondary spreads to lungs from remaining parts of the body. There can exist Small Cell Lung Carcinoma (SCLC) and Non-Small Cell Lung Carcinoma (NSCLC). These lung carcinomas are categorized by the size and appearance of the malignant cells under the microscope. The NSCLC are further classified into squamous cell carcinoma, large cell carcinoma and adenocarcinoma. The SCLC (20% of all cases) is less common, more aggressive and faster than NSCLC (80% of all cases) [https://s3-us-west-1.amazonaws.com/static.cancercommons.org/Handbook_v4_05_electronic+copy.pdf]

A tissue with abnormal growth of cells is called as a tumor. The tumor is classified into malignant (cancerous) and benign (non-cancerous). A benign tumor grows slower and is not harmful to life. It will not spread to other organs. Malignant tumors are life threatening and grow back even after removing it surgically. It also spreads quickly to other organs present in the body. The methods used for effective diagnosis of lung cancer include Computed Tomography (CT) scan, and Magnetic resonance imaging.

2. MEDICAL IMAGE SEGMENTATION

Segmentation is the process of highlighting the boundaries of objects of interests in a given image based on their shapes, locations of the objects, and the depth of each pixel. Medical image segmentation helps in differentiating good tissues of an organ from the other parts of a body and a damaged structure like bone breakage, or growth

of tumor in the brain, breast, etc. Lung segmentation is a technique to the development of automated Computer-Aided Diagnosis (CAD) system for CT slices of the lungs. It is the process of separating the lung region from other anatomical portion of the body in chest CT image.

Earlier segmentation of images have been done by using thresholding, edge detection, region are growing, and morphological operations. Each method has their advantages and limitations. However, manual segmentation performed by domain experts is considered to be the most accurate but is time-consuming. Moreover, semiautomatic segmentation requires minimal user intervention since it is necessary to provide suitable inputs and parameters to facilitate the accuracy of segmentation. Since automatic segmentation does not require any user input, it is more complex regarding computation and obtaining accurate results. In applications involving the processing of a large number of images, automatic segmentation may be preferred for obtaining accurate results.

Fuzzy logic (FL) converts fuzzy data into crisp values. It involves in the association of data to more than one category. Other soft computing algorithms can be combined with fuzzy logic for lung segmentation.

Artificial Neural Network (ANN) is the simulation of the functionality of the human brain. The working of ANN is realized by implementing the mathematical representation of ANN through programming. The implementation of ANN for an application can be done by using one of the supervised/unsupervised/recurrent algorithms. ANN maps sets of input-output data. Two phases of implementation of ANN for an application is required. In phase-1, connection weights are updated by mapping input-output data. In phase-2, outputs are obtained when an input is given. ANN can be used for lung segmentation.

There are some semi-automated, pixel-based methods for segmenting CT images. In pixel-based methods, the initial process is to eliminate fat tissue and bones present in the CT lung images. The lung parenchyma has a very low density and low intensity of pixels in the CT scan. This property is utilized for the process of separating two lungs from the surrounding tissue. A technique commonly used in the semiautomatic segmentation of CT images is gray-level thresholding. By knowing the X-ray attenuation of different tissues, it can be easily identified by differentiating the pixels within a specified range of gray-level. Histogram analysis is used to set threshold values. The set threshold is combined with seeded region-growing so that the pixels are included in the segmentation region. The major drawback behind the pixel-based segmentation is that the neighboring pixels are not considered while assigning segmentation to each and every pixel.

Lee et. al., 2010, implemented an ensemble classification based on random forest algorithm for segmenting lungs. Marios et. al., 2010, developed a matched filter based on an adaptive model of the object acquisition and reconstruction process. This approach uses a sum of absolute differences cost function. Michael et. al., 2010, detected pulmonary nodules using genetic algorithm and random subspace method. Murat et. al., 2010, implemented complex-Valued Artificial Neural Network with Complex Wavelet Transform (CWT-CVANN) for the segmentation of lung region on chest CT images. Serhat Ozekes and Onur Osman, 2010, implemented feature extraction system from the lung images. Neural network, support vector machine, naïve Bayes, and logistic regression were used for nodule detection. Temesguen et. al., 2010, implemented segmentation of lung images. They used thresholding with morphological processing to detect and segment nodule candidates simultaneously. Zsolt et. al., 2010, analyzed the performance of a commercial computer-aided diagnosis software in the detection of pulmonary nodules in original and energy-subtracted chest radiographs.

Seongjin et. al., 2011, implemented gray-level co-occurrence matrix (GLCM) texture analysis for identifying nodules. Stefano et. al., 2011, implemented local shape analysis of the initial segmentation making use of 3-D geodesic distance map representations for identifying lung nodules. Toshiro et. al., 2011, segmented lung images by separating lung parenchyma using diffusion processes. Using Euclidean distance transformation of the foreground, nodules are identified. Xiuhua et. al., 2011, compared original CT images versus enhanced CT images based on the wavelet transform to identify nodules.

Karthikeyan and Ramadoss, 2012, implemented Fuzzy *c*-Means clustering to segment the lungs. Lee et. al., 2012, described different lung segmentation algorithms. Marco et. al., 2012, used labelling method and atlas for lymph node identification. Rahil et. al., 2012, implemented the genetic algorithm and Type-2 fuzzy system for nodule detection in lungs.

Jinke Wang and Haoyan Guo, 2016, implemented skin boundary detection, rough segmentation of lung contour, and pulmonary parenchyma refinement for lung segmentation. Wenjun et. al., 2016, segmented lung image using hierarchical Dirichlet process.

The thresholding based methods depend mostly on the brightness constant called threshold value of the pixels in the original image. This thresholding based method works well in images which have a bimodal distribution. These threshold-based methods perform well in chest CT scans of patients with normal lungs.

3. LUNG NODULE DETECTION

Lung nodule detection involves in identifying the external or internal growth of unwanted tissue in and around the lungs. The nodules have to be detected to save the patients from loss of life. The contrast between lung and neighbor tissues is the basis for most lung segmentation methods.

Various systems have been designed in the past to detect the nodules present in the CT lung images. Serhat, et. al., 2010 proposed feed-forward Neural Networks, Support Vector Machines (SVM), Naïve Bayes (NB) and Logistic Regression (LR) methods for segmentation of lung images.

4. DATA COLLECTION

The existing Lung image database from early lung cancer action program (ELCAP-<http://www.ielcap.org/>) and lung image database consortium (LIDC-<http://imaging.cancer.gov/programsandresources/informationssystemslidc>) public image database provides a set of CT images for comparing different computer-aided diagnosis (CAD) systems. The database consists of an image set of 50 low-dose documented whole-lung CT scans for detection. The whole-lung dataset consists of 50 CT scans obtained in a single breath hold with a 1.25 mm slice thickness. The locations of nodules detected by the radiologist are also provided. Case id is W0001-1 till W0001-50. Image size is 512×512 in the *x-y* direction. The number of slices (276 or 280 or 249 or 243 or 273) varies for each case id. The resolution in the slice varies from 0.59×0.59 , or, 0.62×0.62 , or, 0.67×0.67 , or, 0.7×0.7 , and 0.76×0.76 . Similarly, the numbers of slices that contain nodules also vary in each case id.

5. ROTATIONAL WAVELET GABOR FILTER

Lung image segmentation helps in identifying nodules in the lungs. The Gabor wavelets are used for image analysis especially in feature extraction. Roughness features are extracted at different resolutions using Gabor wavelet. The derivatives of first and second at different orientations like 0° , 45° , 90° and 135° and scales such as 1, 2 and 4 are used for the feature extraction.

Preprocessing The Image

Noise is removed by preprocessing the image. To achieve this Gaussian function is used as given by equation (1).

$$\phi(x, y, s) = \exp \left\{ \frac{-x^2 + y^2}{2s^2} \right\} \quad (1)$$

where,

x, y – directions

s – scale

Feature Extraction

Feature extraction represents important information an image that is different from another image. Directional and percentage energy feature functions are used for extracting features. In the directional roughness feature the first order partial derivative function along x and y are given as follows:

Along x -direction (0°)

$$W_0(x, y, s) = \frac{\partial\phi(x, y, s)}{\partial x} = \frac{-x}{s} \exp\left\{\frac{-x^2 + y^2}{2s^2}\right\} \quad (2)$$

Along y -direction (90°)

$$W_{90}(x, y, s) = \frac{\partial\phi(x, y, s)}{\partial y} = \frac{-y}{s} \exp\left\{\frac{-x^2 + y^2}{2s^2}\right\} \quad (3)$$

Gradient component is obtained by convolution of the image with the filters as given in equation (4) and (5).

$$W_0(x, y, s) \times f(x, y) = \frac{\partial\phi(x, y, s)}{\partial x} \times f(x, y) \quad (4)$$

$$W_{90}(x, y, s) \times f(x, y) = \frac{\partial\phi(x, y, s)}{\partial y} \times f(x, y) \quad (5)$$

The linear combinations of equations 4 and 5 is used for calculations of gradient other than 0° and 90° as given in equation (6).

$$W_\theta(x, y, s) \times f(x, y) = [W_0(x, y, s) \times f(x, y)] \cos \theta + [W_{90}(x, y, s) \times f(x, y)] \sin \theta \quad (6)$$

where, θ is the directional angle.

Partial derivative with a second order for the direction ($0^\circ, 90^\circ$) is obtained by partial differentiation of $W_0(x, y, s)$ on x as given by equation (7).

$$W_{0,90}(x, y, s) = \frac{\partial^2\phi(x, y, s)}{\partial x\partial y} = \frac{xy}{s^4} \exp\left\{\frac{-x^2 + y^2}{2s^2}\right\} \quad (7)$$

The direction ($0^\circ, 0^\circ$) with second order is obtained by differentiation of $W_0(x, y, s)$ on x as given by equation (8).

$$W_{0,0}(x, y, s) = \frac{\partial^2\phi(x, y, s)}{\partial^2 x} = \left(\frac{x^2}{s^4} - \frac{1}{s^2}\right) \exp\left\{\frac{-x^2 + y^2}{2s^2}\right\} \quad (8)$$

The direction ($90^\circ, 90^\circ$) is obtained by differentiation of $W_{90}(x, y, s)$ on y as given by equation (9).

$$W_{90,90}(x, y, s) = \frac{\partial^2\phi(x, y, s)}{\partial^2 y} = \left(\frac{y^2}{s^4} - \frac{1}{s^2}\right) \exp\left\{\frac{-x^2 + y^2}{2s^2}\right\} \quad (9)$$

Linear combination of the equations (7) and (8) filters the image in other angles.

$$W_{\theta, \theta + 90}(x, y, s) \times f(x, y) = [W_{0, 90}(x, y, s) \times f(x, y)] \times \cos 2\theta + 0.5 \times \{[W_{0, 0}(x, y, s) \times f(x, y)] - [W_{90, 90}(x, y, s) \times f(x, y)] \sin 2\theta \} \quad (10)$$

The gradient component along any directions is found by using the equations (9) and (10). The two wavelet transforms of a function $f(x, y)$ at scale s and direction θ are calculated and it is given by equation (11) and (12).

$$W_1 T_f^\theta(x, y, s) = W_0(x, y, s) \times f(x, y) \quad (11)$$

$$W_2 T_f^\theta(x, y, s) = W_{\theta, \theta + 90}(x, y, s) \times f(x, y) \quad (12)$$

where,

$W_1 T_f^\theta(x, y, s)$ – is the first derivative wavelet

$W_2 T_f^\theta(x, y, s)$ – is the second derivative wavelet

The directional roughness features ($R_{s,i}^\theta$): The mean of a window 9×9 using the equations (11) and (12) give directional roughness. The wavelet with the maximum value of roughness is selected as given in equation (13).

$$R_{s,i}^\theta \approx \langle \max |W_i T_f^\theta(u, v, s)| \rangle_{N \times N} \quad (13)$$

$\langle \rangle_{N \times N}$ is the mean of $N \times N$ window.

' i ' represents first, second derivatives.

Percentage of Energy Feature: The effect of roughness depends on the relative lung image energy between different directions. The energy computed in direction θ using an 's'-scale wavelet is given by equation (14).

$$E_{s,i}^\theta \approx \langle |W_i T_f^\theta(x, y, s)| \rangle_{N \times N} \quad (14)$$

Total Energy: The total energy at scale 's' is obtained by equation (15).

$$R_{s,i}^\theta \approx \sum_{\theta} \approx \langle |W_i T_f^\theta(x, y, s)| \rangle_{N \times N} \quad (15)$$

Percentage of Energy: The percentage of energy feature computed in direction θ and scale 's' is given by equation (16).

$$\text{Per}_{s,i}^\theta = \frac{E_s^\theta}{E_s^{\text{total}}} \quad (16)$$

where,

E_s^θ – is the energy computed in direction θ

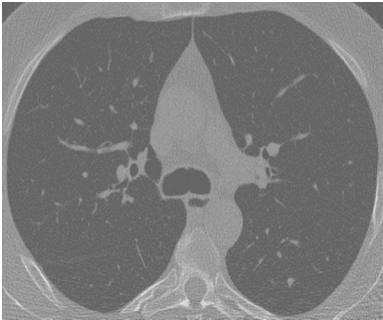
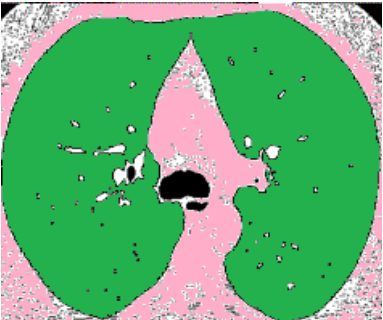

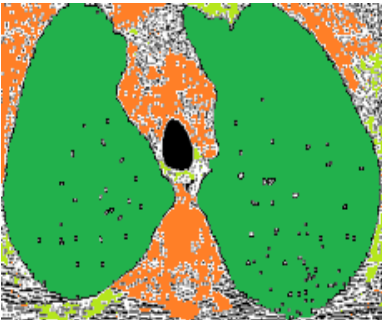

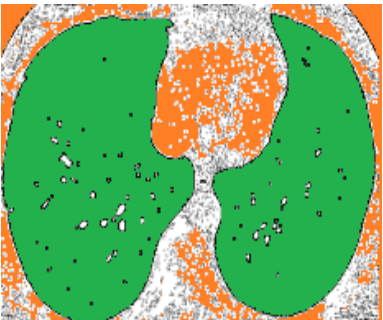
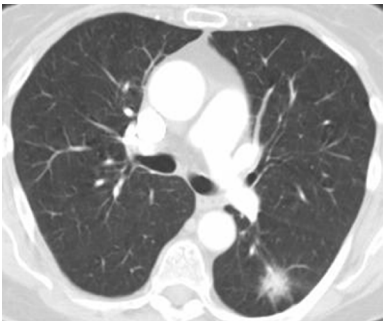
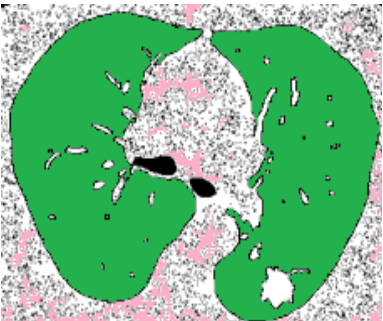
E_s^{total} – is the total energy

The percentage of energy $\text{Per}_{s,i}^\theta$ is insensitive to the absolute image illumination and contrast changes.

6. RESULTS AND DISCUSSIONS

Table 1 presents four different lung images taken from one patient. Each lung image is preprocessed and segmented by using the Gabor filter. The size of the window used for segmentation is 9×9 . Each segmented image contains lungs shown in the dark green color (artificially colored). The remaining portions of the image are colored with different appearances. The white patch inside the green colored portion can be a normal tissue or nodules of benign and malignant. Presence of nodules is confirmed with statistical methods and template matching.

Table 1
Segmented lung images

<i>Original Lung image</i>	<i>Segmented Lung image</i>
	
	
	
	

Segmentation accuracy estimation: Pixel criteria is used for evaluating the segmentation accuracy as given by equation (17).

$$S(\%) = (N_p/P_T) \times 100 \tag{17}$$

where,

S is the segmentation accuracy

N_p is the number of pixels segmented

P_T is the total number of pixels segmented as per the reference image.

Table 2
Accuracy based on pixels segmented

<i>Image Number</i>	P_T	P_T (Ground truth)	<i>S (%)</i>
79	459	465	98.7
81	545	570	95.61
180	629	643	97.82
201	457	471	97.02
			Average: 97.25

Table 2 presents the segmentation accuracy based on the number of pixels segmented. The size of the lung portions in each image varies as the image number increases. Due to this the number of pixels segmented varies. The accuracy of segmentation is based on the clear demarcation of the lung portions from the background of the image. Out of the four images used for segmentation, the minimum segmentation accuracy obtained is 95.61% and the maximum segmentation accuracy obtained is 97.82%. The percentage value varies as the size of the window changes. The optimal size of the window chosen is 9×9 .

7. CONCLUSION

This paper has implemented rotational wavelet Gabor wavelet filter for segmentation of lung image. Directional features at different orientations, and energy features along each direction are computed using the first order and second order partial derivatives of the Gabor wavelet. The size of the window used for the calculation of the features contributes to the accuracy of segmentation.

REFERENCES

- [1] Jinke Wang and Haoyan Guo, (2016), Automatic Approach for Lung Segmentation with Juxta-Pleural Nodules from Thoracic CT Based on Contour Tracing and Correction, Vol. 2016, pp. 1-13.
- [2] Karthikeyan C. and B. Ramadoss, (2012), Segmentation Algorithm for CT Images using Morphological Operation and Artificial Neural Network International Journal of Signal Processing, Image Processing and Pattern Recognition, Vol. 5, No. 2, pp. 115-122.
- [3] Lee S.L.A., Kouzani A.Z., and Hu-E.J., (2012), Automated detection of lung nodules in CT images: a review, Machine Vision and Applications, Vol. 23, Issue 1, pp. 151-163.
- [4] Lee S.L.A., Kouzania A.Z., Hub E.J., (2010), Random forest-based lung nodule classification aided by clustering, Computerized Medical Imaging and Graphics, Vol. 34, pp. 535-542.
- [5] Marco Feuerstein, Ben Glocker, Takayuki Kitasaka, Yoshihiko Nakamura, Shingo Iwano, and Kensaku Mori, (2012), Mediastinal atlas creation from 3D chest CT images: application to automated detection and station mapping of lymph nodes, Medical Image analysis, Vol. 16, pp. 63-74.
- [6] Marios A. Gavrielides, Rongping Zeng, Lisa M. Kinnard, Kyle J. Myers, and Nicholas Petrick, (2010), Information Theoretic approach for analyzing bias and variance in lung nodule size estimation with CT:A phantom study, IEEE Transactions On Medical Imaging, Vol. 29, No. 10, pp. 1795-1807.

- [7] Michael C. Lee, Lilla Boroczky, Kivilcim Sungur-Stasik, Aaron D. Cann, Alain C. Borczuk, Steven M. Kawut, and Charles A. Powell, (2010), Computer aided diagnosis of pulmonary nodules using a two step approach for feature extraction and classifier ensemble construction, *Artificial Intelligence in Medicine*, Vol. 50, Issue 1, pp. 43-53.
- [8] Murat CEYLAN, Yuksel OZBAY, O. Nuri UC, AND, Erkan YILDIRIM, (2010), A novel method for lung segmentation on chest CT images: complex-valued artificial neural network with complex wavelet transform, *Turkey Journal of Electrical Engineering and Computer Science*, Vol. 18, No. 4, pp. 613-623.
- [9] Rahil Hosseini, Salah D. Qanadli, Sarah Barman, Mahdi Mazinani, Tim Ellis, and Jamshid Dehmeshki, (2012), An Automatic Approach for Learning and Tuning Gaussian Interval Type-2 Fuzzy Membership Functions Applied to Lung CAD Classification System, *IEEE Transactions on Fuzzy Systems*, Vol. 20, Issue 2, pp. 224-234.
- [10] Seongjin Park, Bohyoung Kim, Jeongjin Lee, Jin Mo Goo, and Yeong-Gil Shin, (2011), GGO Nodule Volume-Preserving Non rigid Lung Registration Using GLCM Texture Analysis, *IEEE Transactions On Biomedical Engineering*, Vol. 58, No. 10, pp. 2885-2894.
- [11] Serhat Ozekes & Onur Osman, (2010), Computerized Lung Nodule Detection Using 3D Feature Extraction and Learning Based Algorithms, *Journal of Med Syst*, Vol. 34, pp. 185-194.
- [12] Stefano Diciotti, Simone Lombardo, Massimo Falchini, Giulia Picozzi, and Mario Mascalchi, (2011), Automated Segmentation Refinement of Small Lung Nodules in CT Scans by Local Shape Analysis, *IEEE Transactions On Biomedical Engineering*, Vol. 58, No. 12, pp. 3418-3428.
- [13] Temesguen Messay, Russell C. Hardie, and Steven K. Rogers, (2010), A new computationally efficient CAD system for pulmonary nodule detection in CT imagery, *Medical Image Analysis*, Vol. 14, Issue 3, pp. 390-406.
- [14] Toshiro Kubota, Anna K. Jerebko, Maneesh Dewan, Marcos Salganicoff, and Arun Krishnan, (2011), Segmentation of pulmonary nodules of various densities with morphological approaches and convexity models, *Medical Image Analysis*, Vol. 15, Issue 1, pp. 133-154.
- [15] Wenjun Cheng, Luyao Ma, Tiejun Yang, Jiali Liang, and Yan Zhang, (2016), Joint Lung CT Image Segmentation: A Hierarchical Bayesian Approach, *PLOS ONE*, pp. 1-13.
- [16] Xiuhua Guo, Xiangye Liu, Huan Wang, Zhigang Liang, Wei Wu, Qian He, Kuncheng Li, and Wei Wang, (2011), Enhanced CT images by the wavelet transform improving diagnostic accuracy of Chest nodules, *Journal of Digital Imaging*, Vol. 24, Issue 1, pp. 44-49.
- [17] Zsolt Szucs-Farkas, Michael A. Patak, Seyran Yuksel-Hatz, Thomas Ruder, and Peter Vock, (2010), Improved detection of pulmonary nodules on energy subtracted chest radiographs with a commercial computer aided diagnosis software: comparison with human observer, *European Radiology*, Vol. 20, Issue 6, pp. 1289-1296.

